

# AdaTSQ: Pushing the Pareto Frontier of Diffusion Transformers via Temporal-Sensitivity Quantization

Shaoqiu Zhang<sup>\* 1</sup> Zizhong Ding<sup>\* 1</sup> Kaicheng Yang<sup>1</sup> Junyi Wu<sup>1</sup> Xianglong Yan<sup>1</sup> Xi Li<sup>2</sup> Bingnan Duan<sup>2</sup>  
 Jianping Fang<sup>2</sup> Yulun Zhang<sup>† 1</sup>

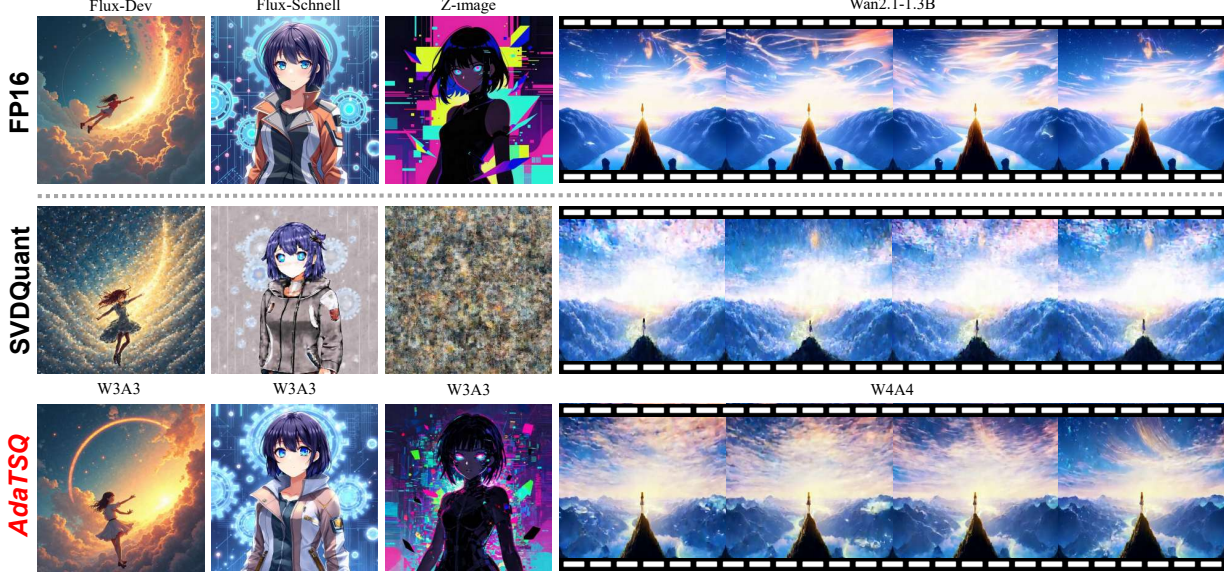


Figure 1. Visual comparison of AdaTSQ with FP16 and SVDQuant (Li\* et al., 2025) under different low-bit quantization settings. The comparison includes three text-to-image models (Flux-Dev, Flux-Schnell, Z-Image) and one text-to-video model (Wan2.1-1.3B).

## Abstract

Diffusion Transformers (DiTs) have emerged as the state-of-the-art backbone for high-fidelity image and video generation. However, their massive computational cost and memory footprint hinder deployment on edge devices. While post-training quantization (PTQ) has proven effective for large language models (LLMs), directly applying existing methods to DiTs yields suboptimal results due to the neglect of the unique temporal dynamics inherent in diffusion processes. In this paper, we propose **AdaTSQ**, a novel PTQ framework that pushes the Pareto frontier of efficiency and quality by exploiting the temporal sensitivity of DiTs. First, we propose a Pareto-aware timestep-dynamic bit-width allocation strategy. We model the quantization policy search as a constrained pathfinding problem. We utilize a beam search algorithm guided by end-to-end recon-

struction error to dynamically assign layer-wise bit-widths across different timesteps. Second, we propose a Fisher-guided temporal calibration mechanism. It leverages temporal Fisher information to prioritize calibration data from highly sensitive timesteps, seamlessly integrating with Hessian-based weight optimization. Extensive experiments on four advanced DiTs (*e.g.*, Flux-Dev, Flux-Schnell, Z-Image, and Wan2.1) demonstrate that AdaTSQ significantly outperforms state-of-the-art methods like SVDQuant and ViDiT-Q. Our code will be released at <https://github.com/Qiushao-E/AdaTSQ>.

## 1. Introduction

The landscape of generative AI has been fundamentally reshaped by Diffusion Transformers (DiTs) (Peebles & Xie, 2023a;b; Bao et al., 2023; Gao et al., 2023; Ma et al., 2024; Lu et al., 2024; Crowson et al., 2024), which have supplanted traditional U-Net architectures (Rombach et al., 2022a; Saharia et al., 2022; Wu et al., 2025b) to establish new state-of-the-art (SOTA) benchmarks in high-fidelity image and video synthesis. Representative models, such as Flux (Labs et al., 2025), Z-Image (Team, 2025; Jiang et al.,

<sup>\*</sup>Equal contribution <sup>†</sup>Shanghai Jiaotong University  
<sup>2</sup>Meituan, China. Correspondence to: Yulun Zhang <yulun100@gmail.com>.

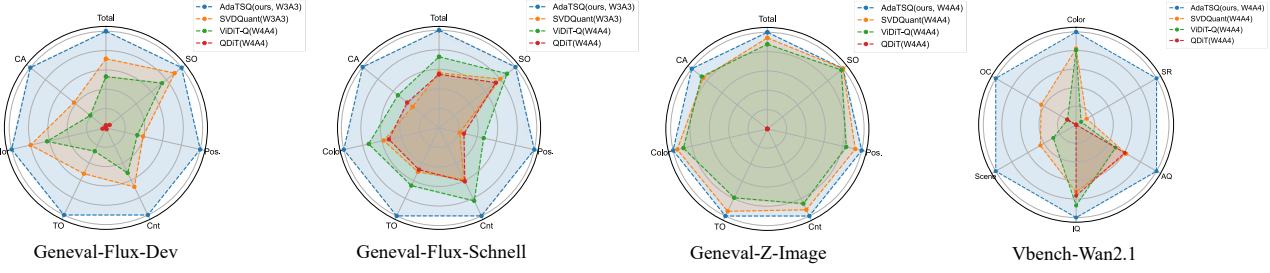


Figure 2. Holistic Performance Comparison. Radar charts comparing AdaTSQ (Blue) with baselines across four DiT models. Axes denote normalized metrics for fidelity, alignment, and consistency. AdaTSQ consistently achieves the largest coverage area, indicating superior comprehensive performance across all modalities and sampling schedules.

2025; Liu et al., 2025a), and Wan2.1 (Wan et al., 2025), demonstrate unparalleled capabilities in generating coherent, photorealistic content. However, this performance comes with substantial computational overhead. Unlike single-pass language models, DiTs require iterative denoising timesteps to generate videos or images, and when combined with the massive parameter count and the quadratic complexity of self-attention mechanisms, the inference cost becomes prohibitive. This immense memory footprint and latency impede their deployment on resource-constrained edge devices and severely limit their applicability in real-time scenarios.

To mitigate these costs, Post-Training Quantization (PTQ) offers a lightweight alternative to expensive Quantization-Aware Training (QAT). In Large Language Models (LLMs), methods like GPTQ (Frantar et al., 2022), AWQ (Lin et al., 2024b), FlatQuant (Sun et al., 2024), QuaRot (Ashkboos et al., 2024), and DuQuant (Lin et al., 2024a) have successfully achieved 4-bit quantization by handling activation outliers. However, these methods focus on static or token-wise distributions. This raises a pivotal question: *Can these text-centric recipes be directly transferred to the temporally dynamic Diffusion Transformers?*

Unfortunately, the answer is negative. Directly applying LLM methods degrades quality by overlooking the unique temporal dynamics of diffusion. Recent DiT-specific attempts also fall short. ViDiT-Q (Zhao et al., 2025) uses rotation but relies on suboptimal static Min-Max weight quantization. SVDQuant (Li\* et al., 2025) employs low-rank decomposition but treats all timesteps uniformly, ignoring varying sensitivities. Similarly, S<sup>2</sup>Q-VDiT (Feng et al., 2025) and others (Liu et al., 2025b; Li et al., 2025; Yang et al., 2025) neglect the critical temporal dimension.

To address these limitations, we argue that the quantization paradigm for DiTs must evolve from static to temporally dynamic. Our motivation stems from two fundamental observations illustrated in Figure 4. First, as shown in the Fisher heatmap (Fig. 4a), the sensitivity of DiT layers to quantization noise is highly non-uniform, exhibiting distinct phases where early steps govern high-level structure and later steps refine details. Second, the activation distributions

shift drastically across the temporal axis (Fig. 4b). These findings imply that a uniform bit-width assignment is inherently suboptimal, as it wastes bit-budget on insensitive denoising steps while starving critical ones, and fails to adapt to the evolving activation statistics.

Based on this finding, we propose AdaTSQ, a unified framework that harmonizes temporal dynamics with quantization efficiency. First, to tackle the combinatorial complexity of assigning bit-widths across varying timesteps, we propose **Pareto-aware timestep-dynamic allocation strategy**. Instead of relying on computationally expensive ILP solvers or manual heuristics, we formulate the allocation as a constrained pathfinding problem. By employing an efficient beam search, we navigate the trade-off space to identify the Pareto-optimal bit-width trajectory, minimizing reconstruction error while strictly adhering to average bit-rate constraints. Second, for weight quantization, we move beyond uniform data calibration by proposing the **Fisher-guided calibration mechanism**. We derive temporal importance scores from Fisher Information to dynamically re-weight the calibration data. This mechanism ensures that the Hessian-based optimization (Frantar et al., 2022) explicitly prioritizes minimizing errors in the most sensitive timesteps, effectively steering quantization noise away from the critical path of the diffusion process.

In summary, our contributions are:

- We propose **AdaTSQ**, a novel PTQ framework that integrates Pareto-aware dynamic allocation strategy and Fisher-guided calibration to exploit the temporal heterogeneity of DiTs’ Quantization.
- We propose a Pareto-aware timestep-dynamic allocation strategy. It solve the constrained pathfinding formulation via beam search to optimally distribute activation bit-budgets across timesteps
- We develop a Fisher-guided temporal calibration strategy to re-weight data, ensuring Hessian-based solvers prioritize accuracy in critical denoising steps.
- Extensive experiments demonstrate the effectiveness of AdaTSQ on Flux, Wan2.1, and Z-Image (Figure 2). We achieve robust W3A3 generation on image models and high-fidelity W4A4 performance on video models.

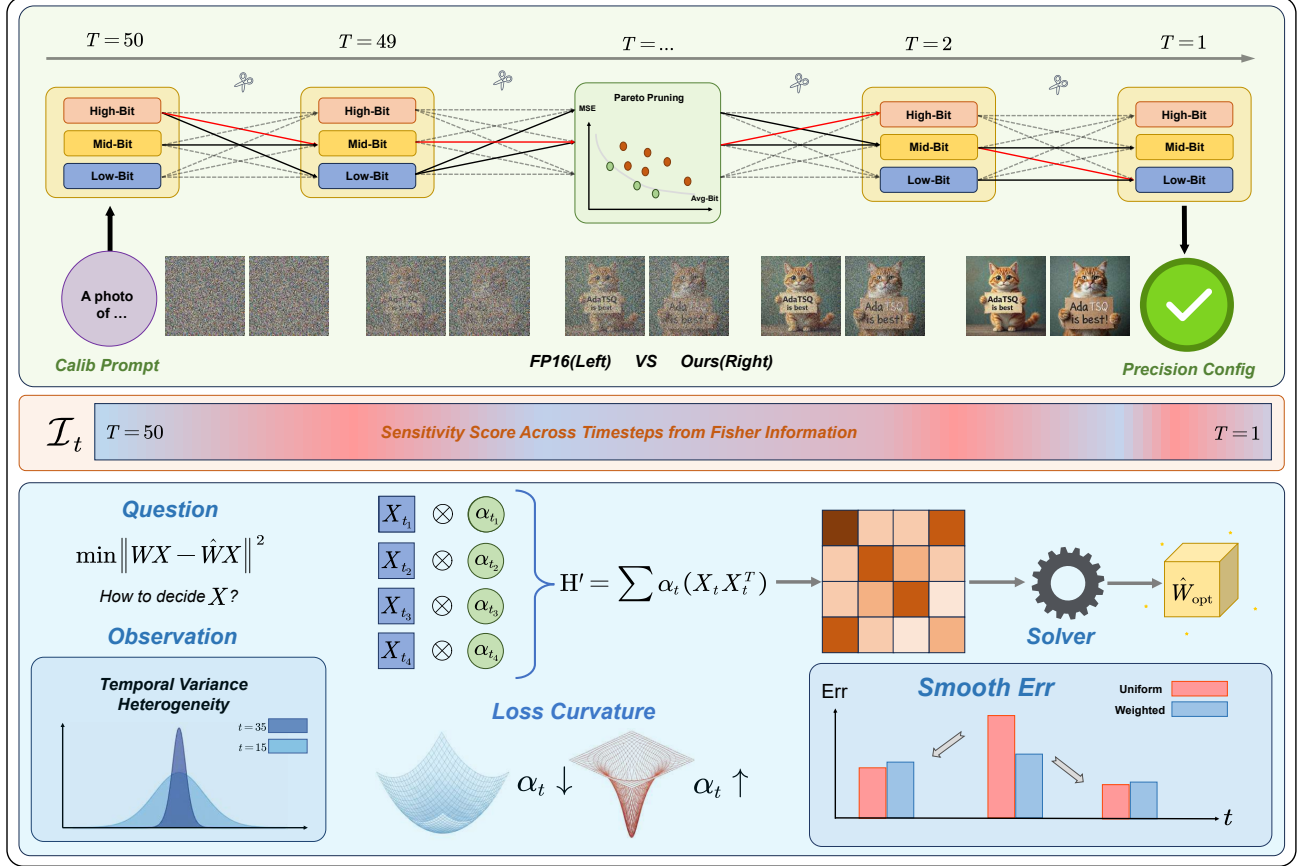


Figure 3. Overview of the **AdaTSQ** framework. The upper panel illustrates the **Pareto-aware Timestep-Dynamic Allocation**, which employs beam search to find the optimal bit-width schedule. The lower panel depicts the **Fisher-Guided Temporal Calibration**, which leverages temporal sensitivity to re-weight the Hessian for risk-aware weight optimization.

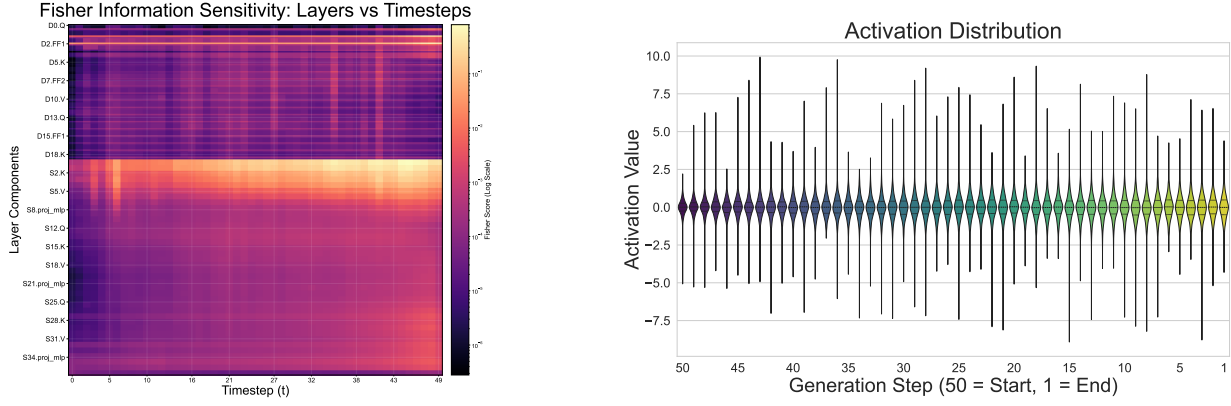
## 2. Related Works

### 2.1. Diffusion Transformers

Diffusion Probabilistic Models (DPMs) (Ho et al., 2020; Song et al., 2021) have emerged as the dominant framework for high-fidelity generative tasks. Early approaches, such as Latent Diffusion Models (LDMs) (Rombach et al., 2022b), typically relied on convolutional U-Net architectures. Recently, the field has decisively shifted towards Diffusion Transformers (DiTs) (Peebles & Xie, 2023a;b; Bao et al., 2023). By adopting a Transformer backbone, DiTs leverage superior scalability and global attention mechanisms to handle complex multi-modal data. This architecture now underpins leading text-to-image and text-to-video models, including Wan2.1 (Wan et al., 2025), Z-image (Team, 2025; Jiang et al., 2025; Liu et al., 2025a), and Flux (Labs et al., 2025). Notably, Flux employs Flow Matching (Lipman et al., 2023), which simplifies the generative process with straighter ODE trajectories and offers potential advantages in training stability. However, despite these improvements, the massive parameter counts and the inherently iterative nature of DiTs result in prohibitive computational costs. This creates an urgent need for efficient compression techniques.

### 2.2. Quantization

Post-Training Quantization (PTQ) has become the standard for compressing large-scale models. In the LLM domain, methods like GPTQ (Frantar et al., 2022), AWQ (Lin et al., 2024b), SmoothQuant (Xiao et al., 2023), QuaRot (Ashkboos et al., 2024), FlatQuant (Sun et al., 2024), and DuQuant (Lin et al., 2024a) successfully pushing the limits to 4 bits. However, transferring these recipes to DiTs is non-trivial. Unlike LLMs, DiTs exhibit drastic temporal shifts in activation distributions (Zhao et al., 2025). Early diffusion quantization focused on U-Nets (Li et al., 2023; Shang et al., 2023), but attention has recently shifted to DiT-specific challenges (Chen et al., 2024; Wu et al., 2024). Advanced methods like ViDiT-Q (Zhao et al., 2025), SVDQuant (Li\* et al., 2025), S<sup>2</sup>Q-VDiT (Feng et al., 2025), and others (Li et al., 2025; Wu et al., 2025a; Liu et al., 2025b) achieve 4-bit quantization via rotation or decomposition. Yet, a critical gap remains. These methods enforce uniform bit-widths or rely on heuristic rules, failing to exploit the varying sensitivity of different denoising phases. In contrast, our work propose a theoretically grounded, Pareto-optimal strategy to allocate bit-budgets across the temporal dimension.



(a) Fisher Sensitivity Heatmap

(b) Activation Distribution Shift

Figure 4. Temporal Heterogeneity in DiTs. (a) Normalized Fisher Information reveals that layer sensitivity varies drastically across different phases of the denoising process (e.g., structure formation vs. texture refinement). (b) Violin plots illustrate significant shifts in activation distributions across timesteps. These observations collectively motivate our timestep-dynamic quantization strategy.

### 3. Method

#### 3.1. Motivation: The Temporal Heterogeneity of DiTs

The core premise of PTQ methods is that layer sensitivity is relatively static or dependent solely on input content. However, in diffusion models, the input distribution evolves drastically over time, shifting from pure Gaussian noise to structured data. This raises a fundamental hypothesis:

*Does the sensitivity of a DiT layer to quantization noise remain constant during the denoising process?*

To answer this, we employ Fisher Information as a theoretically grounded metric for sensitivity. For a given layer  $l$  with weights  $\mathbf{W}_l$ , the Fisher Information at timestep  $t$  can be approximated by the expected squared gradients of the loss  $\mathcal{L}$  with respect to the weights:

$$\mathcal{I}_{t,l} = \mathbb{E}_{\mathbf{x}_t \sim \mathcal{D}_t} \left[ \left( \frac{\partial \mathcal{L}(\mathbf{x}_t)}{\partial \mathbf{W}_l} \right)^2 \right]. \quad (1)$$

Intuitively, a higher  $\mathcal{I}_{t,l}$  indicates that a small perturbation (quantization noise) in layer  $l$  at timestep  $t$  will cause a significant increase in the final task loss.

**Observation.** We visualize the normalized Fisher scores across layers and timesteps in Figure 4a. The heatmap reveals a striking temporal heterogeneity: (1) Layer Variance: In the same timestep, sensitivity varies significantly across different modules. (2) Phase-Dependent Sensitivity: Certain layers are highly sensitive during the early “structure formation” phase but become robust to noise in the later “texture refinement” phase.

**Implication.** This observation invalidates the optimality of uniform quantization. Assigning a static bit-width to all timesteps inevitably leads to a dilemma: it is either wasteful for insensitive steps or destructive for sensitive steps. This necessitates a Timestep-Dynamic Allocation strategy that distributes the bit-budget to where it is most needed.

#### 3.2. Pareto-aware Timestep-Dynamic Allocation

To exploit the temporal heterogeneity revealed in Sec. 3.1, we propose a pareto-aware timestep-dynamic allocation strategy that assigns specific bit-widths to each layer at each timestep. However, the search space is prohibitively large ( $|\mathcal{B}|^{T \times L}$ , where  $|\mathcal{B}|$  is the number of candidate bit-widths). To navigate this space efficiently, we formulate the dynamic bit-width allocation problem as a constrained pathfinding task and solve it via a Pareto-aware beam search.

##### 3.2.1. PROBLEM FORMULATION

Let  $\mathbf{b}_t = \{b_{t,l}\}_{l=1}^L$  denote the bit-width configuration vector for all layers at timestep  $t$ . Our goal is to find a sequence of configurations  $\mathcal{P} = (\mathbf{b}_1, \dots, \mathbf{b}_T)$  that minimizes the cumulative generation error subject to an average bit-width constraint  $B_{\text{target}}$ . We define the step-wise reconstruction error at timestep  $t$  as the MSE between the full-precision output  $\epsilon_\theta(\mathbf{z}_t, t)$  and the quantized output  $\hat{\epsilon}_\theta(\mathbf{z}_t, t; \mathbf{b}_t)$ :

$$\mathcal{L}_{\text{MSE}}(\mathbf{b}_t) = \|\epsilon_\theta(\mathbf{z}_t, t) - \hat{\epsilon}_\theta(\mathbf{z}_t, t; \mathbf{b}_t)\|_2^2. \quad (2)$$

The optimization problem is formulated as:

$$\min_{\mathcal{P}} \sum_{t=1}^T \mathcal{L}_{\text{MSE}}(\mathbf{b}_t) \quad \text{s.t.} \quad \frac{1}{T \cdot L} \sum_{t=1}^T \sum_{l=1}^L b_{t,l} \leq B_{\text{target}}. \quad (3)$$

##### 3.2.2. CANDIDATE GENERATION

Instead of searching bit-widths for each layer, we construct a timestep-specific set of  $M$  candidate configurations  $\mathcal{C}_t = \{\mathbf{c}_t^{(1)}, \dots, \mathbf{c}_t^{(M)}\}$ . Crucially, these candidates are dynamically generated based on the Fisher information  $\mathcal{I}_{t,l}$  at the current timestep. For example, at a sensitive timestep, the clustering algorithm may assign high precision to attention layers. Conversely, at a less sensitive step, it may assign lower precision. This adaptive approach ensures the search space aligns with the evolving sensitivity of the diffusion process, pruning irrelevant paths while enhancing efficiency.

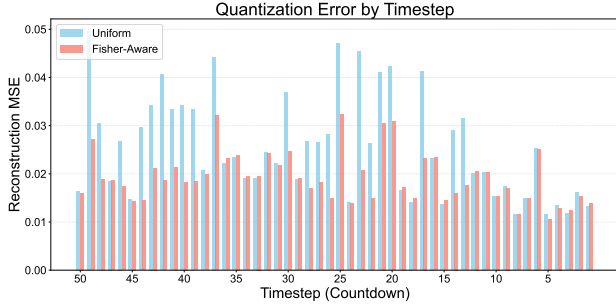


Figure 5. Reconstruction error of transformer.blocks.18.ff.net.2 on Flux-Dev across timesteps. Compared to standard Uniform Calibration (Blue), our Fisher-Guided Calibration (Pink) effectively suppresses quantization noise in high-sensitivity regions, resulting in a smoother and lower risk profile.

### 3.2.3. PARETO-OPTIMAL BEAM SEARCH

We employ a pareto-optimal based beam search algorithm to solve Eq. (3). Unlike standard beam search which keeps the top- $K$  paths based on a single metric, we maintain the Pareto Frontier of paths to balance the trade-off between cumulative error and accumulated bit-cost.

Let  $\mathcal{S}_{t-1} = \{(\text{path}_i, \text{loss}_i, \text{bits}_i)\}_{i=1}^M$  be the set of  $M$  retained paths at step  $t-1$ . For the current step  $t$ , we expand each path by appending every candidate configuration  $\mathbf{c} \in \mathcal{C}_t$ , resulting in  $M \times M$  potential new paths. For each new path  $j$ , we compute:

$$\text{Cumulative Loss: } E_t^{(j)} = E_{t-1}^{(i)} + \mathcal{L}_{\text{MSE}}(\mathbf{c}), \quad (4)$$

$$\text{Cumulative Bits: } B_t^{(j)} = B_{t-1}^{(i)} + \text{avg}(\mathbf{c}). \quad (5)$$

From these  $M^2$  candidates, we select the  $M$  paths that form the Pareto Frontier in the (Bits, Loss) plane. A path  $j$  dominates path  $k$  if  $B_t^{(j)} \leq B_t^{(k)}$  and  $E_t^{(j)} \leq E_t^{(k)}$ . We retain only the non-dominated paths (or the top- $M$  closest to the origin if the frontier size  $> M$ ). This process iterates from  $t=1$  to  $T$ , yielding a final set of paths from which we select the one satisfying  $B_{\text{target}}$ .

### 3.2.4. FINAL SELECTION

Upon completing the beam search at  $t=T$ , we obtain a set of  $M$  Pareto-optimal paths. While the search relies on the cumulative MSE as a computationally efficient proxy, MSE does not always perfectly align with human perception or generative metrics. To ensure the final configuration delivers superior perceptual quality, we perform a lightweight end-to-end generation test on the surviving  $M$  paths. We generate a small batch of samples using each candidate path and evaluate them against task-specific metrics (e.g., CLIP score for text-to-image alignment). The path yielding the best trade-off between the generative metric and the bit-budget is selected as the final quantization policy. This two-stage strategy—efficient MSE-based pruning followed by accurate metric-based selection—drastically reduces the search overhead while guaranteeing optimal generation quality.

### 3.3. Fisher-Guided Temporal Calibration

While Sec. 3.2 resolves activation quantization via timestep-wise bit-width dynamic allocation, weights must remain static across timesteps to avoid memory overhead. Finding a single quantized configuration  $\hat{\mathbf{W}}$  that is robust across all temporal phases is challenging. Existing methods like ViDiT-Q (Zhao et al., 2025) (no calibration) or SVDQuant (Li\* et al., 2025) (uniform calibration) overlook varying temporal sensitivity, often leading to structural artifacts. To address this, we propose **Fisher-Guided Temporal Calibration** (Figure 3). This approach modifies the standard Hessian-based objective to explicitly prioritize critical timesteps based on their Fisher information.

#### 3.3.1. TEMPORAL IMPORTANCE MODELING

To rigorously ground our strategy, we view weight quantization as an Expected Risk Minimization problem. Let  $\mathcal{L}(\theta)$  be the task loss. The loss perturbation due to quantization error  $\Delta \mathbf{W}_l$  can be approximated via Taylor expansion:  $\mathbb{E}[\Delta \mathcal{L}] \approx \frac{1}{2} \Delta \mathbf{W}_l^\top \mathbf{H}_{\mathcal{L},l} \Delta \mathbf{W}_l$ . Standard PTQ approximates the Hessian  $\mathbf{H}_{\mathcal{L},l}$  using input covariance  $\mathbf{X} \mathbf{X}^\top$ , implicitly assuming uniform risk across time.

However, our analysis in Sec. 3.1 reveals that the curvature of the loss landscape varies drastically across time and layers. To align the calibration objective with the true risk, we introduce a layer-wise temporal re-weighting mechanism. We define the temporal importance  $\alpha_{t,l}$  using Fisher Information  $\mathcal{I}_{t,l}$  as a proxy for local curvature magnitude.

To prevent distribution collapse—where a few dominant timesteps suppress others—we employ a Temperature-Scaled Softmax normalization for each layer:

$$\alpha_{t,l} = \frac{\exp(\mathcal{I}_{t,l}/\tau)}{\sum_{t'=1}^T \exp(\mathcal{I}_{t',l}/\tau)}, \quad (6)$$

where  $\tau$  is a temperature hyperparameter. This formulation ensures that each layer focuses on its own most critical timesteps during calibration.

#### 3.3.2. RISK-AWARE HESSIAN CALIBRATION

Incorporating  $\alpha_{t,l}$ , we reformulate the quantization objective to minimize the Temporally Weighted Risk:

$$\min_{\hat{\mathbf{W}}_l} \sum_{t=1}^T \alpha_{t,l} \|\mathbf{W}_l \mathbf{X}_{t,l} - \hat{\mathbf{W}}_l \mathbf{X}_{t,l}\|_2^2. \quad (7)$$

Here,  $\mathbf{X}_{t,l}$  denotes calibration inputs at timestep  $t$ . To solve this efficiently, we derive the Risk-Aware Hessian  $\mathbf{H}'_l$ :

$$\mathbf{H}'_l = \sum_{t=1}^T \alpha_{t,l} (\mathbf{X}_{t,l} \mathbf{X}_{t,l}^\top). \quad (8)$$

This is equivalent to scaling input features  $\mathbf{X}_{t,l}$  by  $\sqrt{\alpha_{t,l}}$  prior to Hessian accumulation. By doing so, we seamlessly inject temporal awareness into standard solvers, effectively warping the optimization landscape to preserve structural integrity where it matters most for each component.

Table 1. Quantization results on GenEval. The best and the second best results are marked with red and blue, respectively.

Model	Method	Bits (W/A)	Single Object	Position	Counting	Two Object	Colors	Color Attribute	Total
FLUX-dev (50 steps)	FP	16/16	0.9844	0.2025	0.7688	0.8232	0.7713	0.4500	0.6667
	Q-DiT	4/4	0.0469	0.0000	0.0094	0.0000	0.0239	0.0025	0.0138
	SmoothQuant	4/4	0.0025	0.0000	0.0031	0.0000	0.0106	0.0000	0.0065
	Quarot	4/4	0.6344	0.0250	0.2938	0.1061	0.3457	0.0500	0.2425
	ViDiT-Q	4/4	0.7094	0.0275	0.3250	0.1465	0.4096	0.0600	0.2797
	SVDQuant	4/4	0.9812	0.1400	0.6100	0.7100	0.6979	0.3000	0.5732
	AdaTSQ (ours)	4/4	0.9812	0.2600	0.6400	0.7700	0.7083	0.3500	0.6183
	SVDQuant	3/3	0.8688	0.0325	0.4250	0.2879	0.5239	0.1225	0.3768
	AdaTSQ (ours)	3/3	0.9562	0.0825	0.6281	0.5480	0.6559	0.2900	0.5270
FLUX-schnell (4 steps)	FP	16/16	0.9969	0.2750	0.6000	0.8838	0.7420	0.4875	0.6642
	Q-DiT	4/4	0.7406	0.0725	0.3781	0.4242	0.4176	0.2075	0.3734
	SmoothQuant	4/4	0.6188	0.0425	0.2719	0.2929	0.3165	0.1425	0.2808
	Quarot	4/4	0.8188	0.1175	0.4719	0.5429	0.5186	0.2750	0.4575
	ViDiT-Q	4/4	0.8875	0.1300	0.5156	0.5859	0.5851	0.2675	0.4953
	SVDQuant	4/4	0.9938	0.2600	0.4500	0.9100	0.7083	0.4200	0.6237
	AdaTSQ (ours)	4/4	0.9969	0.2775	0.6219	0.8939	0.7926	0.4975	0.6801
	SVDQuant	3/3	0.8200	0.1600	0.4656	0.6470	0.5601	0.3725	0.5042
	AdaTSQ (ours)	3/3	0.9969	0.2300	0.5300	0.9200	0.6875	0.4400	0.6341
Z-Image (10 steps)	FP	16/16	1.0000	0.4675	0.7094	0.9066	0.8590	0.5825	0.7542
	Q-DiT	4/4	N/A	N/A	N/A	N/A	N/A	N/A	N/A
	SmoothQuant	4/4	0.0031	0.0000	0.0000	0.0000	0.0000	0.0000	0.0000
	Quarot	4/4	0.9062	0.2500	0.4156	0.5051	0.6915	0.3425	0.5185
	ViDiT-Q	4/4	0.9719	0.4350	0.5844	0.7045	0.7766	0.5325	0.6675
	SVDQuant	4/4	0.9938	0.4850	0.6325	0.8430	0.8332	0.5200	0.7179
	AdaTSQ (ours)	4/4	0.9938	0.5200	0.6812	0.8914	0.8723	0.6125	0.7619
	SVDQuant	3/3	0.0047	0.0000	0.0000	0.0000	0.0000	0.0000	0.0001
	AdaTSQ (ours)	3/3	0.9938	0.4100	0.5500	0.8700	0.8854	0.4545	0.6940

Table 2. Quantization results on VBench. The best and the second best results are marked with red and blue, respectively.

Model	Methods	Bits (W/A)	Imaging Quality	Aesthetic Quality	Motion Smooth.	Dynamic Degree	BG. Consist.	Scene Consist.	Overall Consist.	Subject Consist.
Wan2.1-1.3B (25 steps)	FP	16/16	0.6055	0.5643	0.9558	0.8333	0.9547	0.2863	0.2510	0.9222
	Q-DiT	4/4	0.4302	0.3070	0.9339	N/A	0.9515	N/A	0.0267	0.9062
	SmoothQuant	4/4	0.5266	0.3838	0.8517	N/A	0.9519	N/A	0.0120	0.9000
	Quarot	4/4	0.3840	0.3415	0.9469	0.5833	0.9631	0.0094	0.1283	0.8986
	ViDiT-Q	4/4	0.4893	0.2487	0.9445	N/A	0.9500	N/A	0.0254	0.8760
	SVDQuant	4/4	0.4073	0.3169	0.9485	0.6444	0.9562	0.0203	0.1024	0.9041
	AdaTSQ (ours)	4/4	0.5626	0.5073	0.9510	0.8472	0.9658	0.2253	0.2356	0.9078

## 4. Experiments

### 4.1. Experimental Setup

**Models & Datasets.** We evaluate AdaTSQ on four state-of-the-art DiT architectures, covering diverse modalities and sampling steps: (1) Flux-Dev (50-step) and (2) Flux-Schnell (4-step) (3) Z-Image (10-step) for text-to-image generation; (4) Wan2.1-1.3B (25-step) for text-to-video generation. For quantitative evaluation, we employ Geneval for text-to-image models, measuring semantic alignment and fidelity. For text-to-video models, we use VBench to assess temporal consistency and visual quality.

**Baselines.** We compare AdaTSQ against a comprehensive suite of quantization methods, including: (1) **DiT-specific approaches** such as SVDQuant (Li\* et al., 2025) (current SOTA) and ViDiT-Q (Zhao et al., 2025); (2) **LLM-adapted techniques** like QuaRot (Ashkboos et al., 2024) and SmoothQuant (Xiao et al., 2023), which represent ad-

vanced static PTQ; and (3) **earlier diffusion quantization methods** including Q-DiT (Chen et al., 2024). All baselines are evaluated under their optimal settings.

### 4.2. Main Results

#### 4.2.1. QUANTITATIVE COMPARISON

**Text-to-Image Generation.** Figure 6 presents qualitative results across three text-to-image models, including Flux-dev, Flux-Schnell and Z-Image. Primitive methods like SmoothQuant and Q-DiT fail completely at W4A4, generating mostly pure noise. While QuaRot and ViDiT-Q capture basic outlines at W4A4, they lack fine-grained details. SVDQuant achieves high fidelity at W4A4 but suffers from significant quality degradation when pushed to W3A3. In contrast, AdaTSQ consistently produces high-quality images that are virtually indistinguishable from the FP16 across both W4A4 and the challenging W3A3 settings.

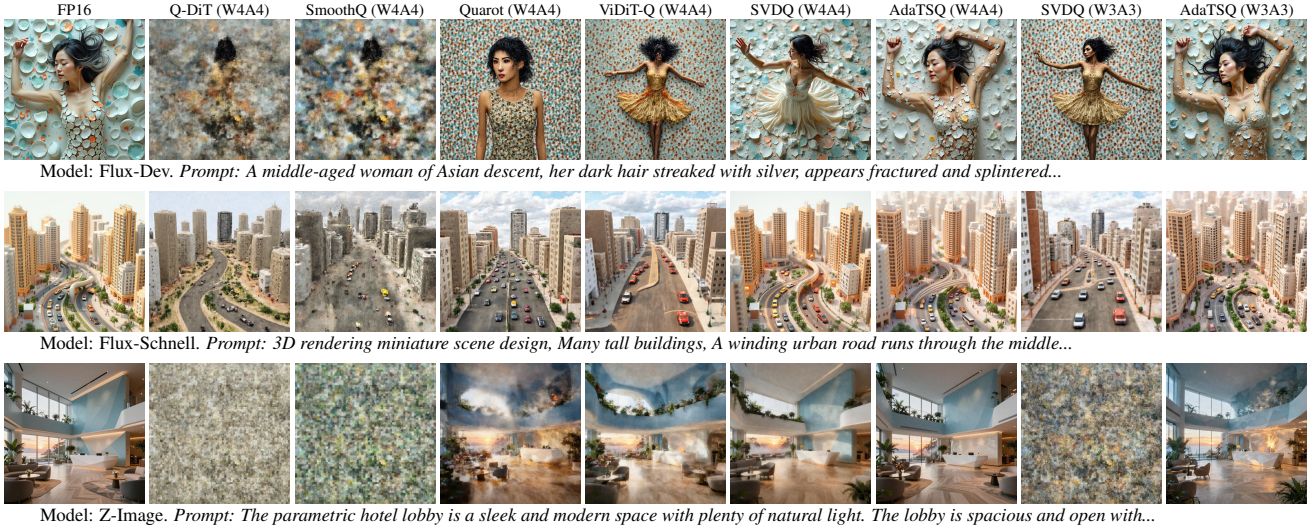
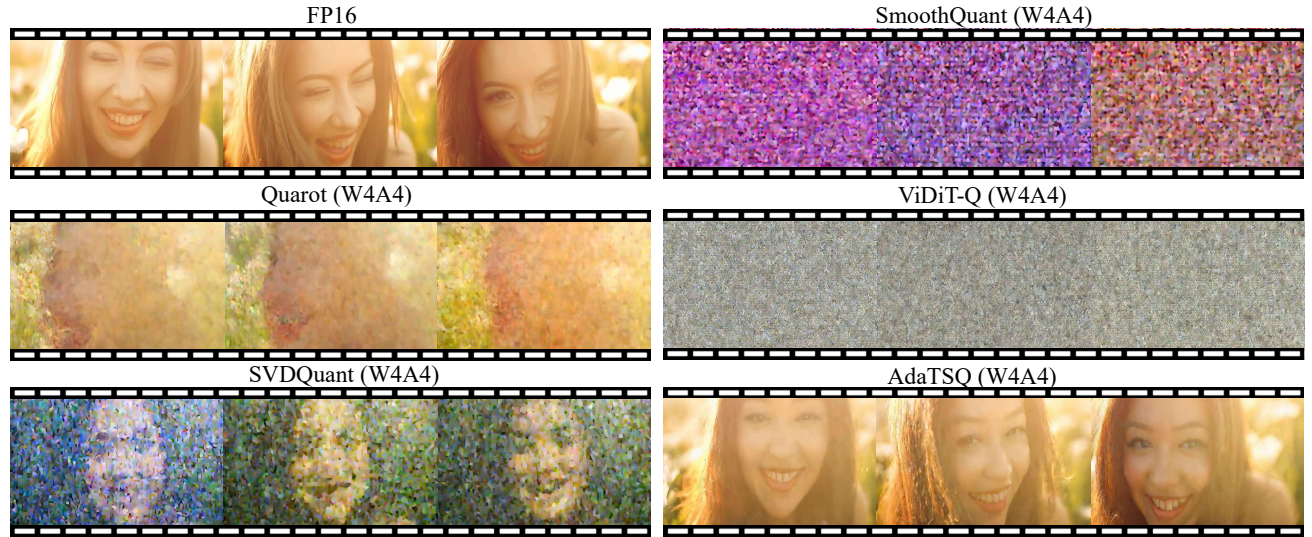


Figure 6. Visual Comparison on Text-to-Image Models. Visual samples from Flux-Dev, Flux-Schnell, and Z-Image generated by AdaTSQ and baselines. AdaTSQ preserves fine-grained details and semantic alignment.



Prompt: *A wide-angle drone shot flying over a jagged mountain range during a sunset. The camera pans down to reveal...*

Figure 7. Visual Comparison on Text-to-Video Model. Visual samples from Wan2.1-1.3B generated by AdaTSQ and baselines.

**Text-to-Video Generation.** In Table 2, on Wan2.1, aggressive W4A4 quantization causes catastrophic failure in several baselines (scores dropping to 0). Notably, SVDQuant struggles with video generation at w4a4. Conversely, AdaTSQ demonstrates superior generalization, achieving faithful results across all metrics, effectively handling the temporal complexity of video generation.

#### 4.2.2. VISUAL COMPARISON

**Text-to-Image Generation.** Figure 6 presents qualitative results across three text-to-image models. Primitive methods like SmoothQuant and Q-DiT fail completely at W4A4, generating mostly pure noise. While QuaRot and ViDiT-Q capture basic outlines at W4A4, they lack fine-grained details. SVDQuant achieves high fidelity at W4A4 but suffers from significant quality degradation when pushed to W3A3. In contrast, AdaTSQ consistently produces high-

quality images that are virtually indistinguishable from the FP16 across both W4A4 and the challenging W3A3 settings.

**Text-to-Video Generation.** Figure 7 visualizes the video generation results of AdaTSQ and baselines. Note that Q-DiT results are omitted as they consist entirely of noise. Under the aggressive W4A4 quantization, both SmoothQuant and ViDiT-Q fail to generate meaningful content, producing only noise; this observation suggests that their scaling-based operations might be ill-suited for the specific characteristics of the Wan model architecture. While QuaRot and SVDQuant manage to preserve basic structural outlines, they still struggle to reconstruct fine-grained details, leading to visually flat outputs. In contrast, AdaTSQ generates videos with remarkably high quality, maintaining both temporal consistency and visual fidelity, thereby mitigating the jitter and distortion observed in low-bit video synthesis.

Table 3. Ablation Study on Flux-Dev (W3A3). We evaluate the contribution of Pareto-aware Allocation (“Pareto”) and Fisher-Guided Calibration (“Fisher Calib”). “Avg Calib” denotes standard GPTQ with uniform temporal weighting.

Method	Single Object	Position	Counting	Two Object	Colors	Color Attribute	Total
1. Baseline (MinMax W)	0.5594	0.0175	0.2688	0.0985	0.3484	0.0500	0.2238
2. + Pareto Alloc	0.8562	0.0725	0.5031	0.3409	0.5771	0.1675	0.4196
3. + Fisher Calib	0.8125	0.0385	0.4719	0.2803	0.4920	0.4191	0.4190
4. + Pareto Alloc + Avg Calib	0.8812	0.0750	0.5717	0.5197	0.5214	0.2272	0.4660
<b>5. AdaTSQ</b>	<b>0.9562</b>	<b>0.0825</b>	<b>0.6281</b>	<b>0.5480</b>	<b>0.6559</b>	<b>0.2900</b>	<b>0.5270</b>



Figure 8. Visual comparison of the ablation study, which is generated by Flux-Dev model under W3A3 setting.

### 4.3. Ablation Studies

To validate the contribution of each component within AdaTSQ, we conduct a comprehensive ablation study on Flux-Dev under the W3A3 setting. The quantitative results are summarized in Table 3, and qualitative comparisons are visualized in Figure 8. The naive baseline (Row 1, using minmax for weight quantization and naive rotation for activation quantization) suffers from severe degradation, producing images with collapsed structures.

**Effect of Pareto-aware Allocation.** Introducing Pareto-aware allocation (Row 2, employing a timestep-wise mixed-precision strategy of 3/4/8-bit) significantly boosts image clarity compared to the baseline by assigning higher precision to sensitive timesteps. However, as shown in Figure 8, semantic alignment remains chaotic, often generating content unrelated to the text prompt.

**Effect of Fisher-Guided Calibration.** Applying Fisher-guided calibration alone (Row 3) partially corrects semantic errors but still exhibits noticeable deviations. This confirms that risk-aware weight optimization—leveraging Fisher information to identify and preserve critical parameters—is crucial for aligning the generation path, but its effectiveness is limited when constrained by fixed bit-widths.

**Synergy and Final Performance.** Combining Pareto allocation with standard average calibration (Row 4) brings structural clarity close to our final method’s result, yet semantic flaws persist due to the lack of sensitivity-aware adjustment (the prompt requires only one bench, but there exists two). The optimal result is consistently achieved by our full method (Row 5). As visualized, AdaTSQ not only maintains high visual clarity but also perfectly resolves semantic alignment constraints, demonstrating that the synergy between dynamic bit allocation and risk-aware calibration is essential for achieving robust generation performance under the extreme W3A3 setting.

Table 4. Theoretical Efficiency on Flux-Dev (12B). Comparison of average bit-width, memory footprint (Model Size), and theoretical computational cost (FLOPs). AdaTSQ achieves  $>5\times$  reduction across all metrics.

Metric	FP16	AdaTSQ	Reduction
Avg. Bit-width	W16A16	W3A3.1	<b>5.16×</b>
Model Size	~24.0 GB	~4.50 GB	<b>5.33×</b>
Norm. FLOPs	1.00×	0.19×	<b>5.16×</b>

### 4.4. Efficiency Analysis

**Search & Inference Efficiency.** A key advantage of AdaTSQ is its minimal overhead. The Pareto-aware beam search is extremely efficient; on a single A100-80GB GPU, finding the optimal mixed-precision policy for the 50-step Flux-Dev model requires only  $\sim 4$  minutes. This negligible one-off cost unlocks substantial theoretical gains, as summarized in Table 4. Based on the searched policy, the bit-width distribution converges to approximately 80% 3-bit, 10% 4-bit, and 10% 8-bit. This results in an effective average bit-width of 3.1 bits, translating to a theoretical **5.16× reduction** in computational FLOPs and **5.33×** in model size and compared to the FP16 baseline.

## 5. Conclusion

We presented **AdaTSQ**, a novel PTQ framework that systematically exploits the temporal heterogeneity of Diffusion Transformers. By quantizing activation with Pareto-aware timestep-dynamic allocation and introducing Fisher-guided temporal weight calibration, AdaTSQ effectively resolves the conflict between static quantization parameters and dynamic activation distributions. Extensive experiments demonstrate that our method achieves state-of-the-art performance, enabling perceptually W4A4 quantization across diverse image and video models. Most notably, we unlock viable W3A3 generation on text-to-image models for the first time, revealing the inherent robustness of image generation models to low-bit compression.

## References

- Ashkboos, S., Mohtashami, A., Croci, M. L., Li, B., Jaggi, M., Alistarh, D., Hoefer, T., and Hensman, J. Quarot: Outlier-free 4-bit inference in rotated llms. *arXiv preprint arXiv:2404.00456*, 2024.
- Bao, F., Nie, S., Xue, K., Cao, Y., Li, C., Su, H., and Zhu, J. All are worth words: A vit backbone for diffusion models. In *CVPR*, 2023.
- Chen, L., Meng, Y., Tang, C., Ma, X., Jiang, J., Wang, X., Wang, Z., and Zhu, W. Q-dit: Accurate post-training quantization for diffusion transformers, 2024.
- Crowson, K., Baumann, S. A., Birch, A., Abraham, T. M., Kaplan, D. Z., and Shippole, E. Scalable high-resolution pixel-space image synthesis with hourglass diffusion transformers. *arXiv preprint arXiv:2401.11605*, 2024.
- Feng, W., Qin, H., Yang, C., Li, X., Yang, H., Li, Y., An, Z., Huang, L., Magno, M., and Xu, Y. S<sup>2</sup>q-vdit: Accurate quantized video diffusion transformer with salient data and sparse token distillation. *arXiv preprint arXiv:2508.04016*, 2025.
- Frantar, E., Ashkboos, S., Hoefer, T., and Alistarh, D. GPTQ: Accurate post-training compression for generative pretrained transformers. *arXiv preprint arXiv:2210.17323*, 2022.
- Gao, S., Zhou, P., Cheng, M.-M., and Yan, S. Masked diffusion transformer is a strong image synthesizer. In *ICCV*, 2023.
- Ho, J., Jain, A., and Abbeel, P. Denoising diffusion probabilistic models. In *NeurIPS*, 2020.
- Jiang, D., Liu, D., Wang, Z., Wu, Q., Jin, X., Liu, D., Li, Z., Wang, M., Gao, P., and Yang, H. Distribution matching distillation meets reinforcement learning. *arXiv preprint arXiv:2511.13649*, 2025.
- Labs, B. F., Batifol, S., Blattmann, A., Boesel, F., Consul, S., Diagne, C., Dockhorn, T., English, J., English, Z., Esser, P., Kulal, S., Lacey, K., Levi, Y., Li, C., Lorenz, D., Müller, J., Podell, D., Rombach, R., Saini, H., Sauer, A., and Smith, L. Flux.1 kontext: Flow matching for in-context image generation and editing in latent space, 2025.
- Li\*, M., Lin\*, Y., Zhang\*, Z., Cai, T., Li, X., Guo, J., Xie, E., Meng, C., Zhu, J.-Y., and Han, S. Svdquant: Absorbing outliers by low-rank components for 4-bit diffusion models. In *ICLR*, 2025.
- Li, X., Liu, Y., Lian, L., Yang, H., Dong, Z., Kang, D., Zhang, S., and Keutzer, K. Q-diffusion: Quantizing diffusion models. In *ICCV*, 2023.
- Li, Z., Li, H., Wu, J., Liu, K., Kong, L., Chen, G., Zhang, Y., and Yang, X. Dvd-quant: Data-free video diffusion transformers quantization. *arXiv preprint arXiv:2505.18663*, 2025.
- Lin, H., Xu, H., Wu, Y., Cui, J., Zhang, Y., Mou, L., Song, L., Sun, Z., and Wei, Y. Duquant: Distributing outliers via dual transformation makes stronger quantized llms. *arXiv preprint arXiv:2406.01721*, 2024a.
- Lin, J., Tang, J., Tang, H., Yang, S., Chen, W.-M., Wang, W.-C., Xiao, G., Dang, X., Gan, C., and Han, S. Awq: Activation-aware weight quantization for llm compression and acceleration. In *MLSys*, 2024b.
- Lipman, Y., Chen, R. T. Q., Ben-Hamu, H., Nickel, M., and Le, M. Flow matching for generative modeling, 2023. URL <https://arxiv.org/abs/2210.02747>.
- Liu, D., Gao, P., Liu, D., Du, R., Li, Z., Wu, Q., Jin, X., Cao, S., Zhang, S., Li, H., and Hoi, S. Decoupled dmd: Cfg augmentation as the spear, distribution matching as the shield. *arXiv preprint arXiv:2511.22677*, 2025a.
- Liu, K., Zhang, S., Kong, L., and Zhang, Y. Clq: Cross-layer guided orthogonal-based quantization for diffusion transformers. *arXiv preprint arXiv:2509.24416*, 2025b.
- Lu, Z., Wang, Z., Huang, D., Wu, C., Liu, X., Ouyang, W., and Bai, L. Fit: Flexible vision transformer for diffusion model. *arXiv preprint arXiv:2402.12376*, 2024.
- Ma, N., Goldstein, M., Albergo, M. S., Boffi, N. M., Vandeneijnden, E., and Xie, S. Sit: Exploring flow and diffusion-based generative models with scalable interpolant transformers. In *ECCV*, 2024.
- Peebles, W. and Xie, S. Scalable diffusion models with transformers, 2023a. URL <https://arxiv.org/abs/2212.09748>.
- Peebles, W. S. and Xie, S. Scalable diffusion models with transformers. *ICCV*, 2023b.
- Rombach, R., Blattmann, A., Lorenz, D., Esser, P., and Ommer, B. High-resolution image synthesis with latent diffusion models. In *CVPR*, 2022a.
- Rombach, R., Blattmann, A., Lorenz, D., Esser, P., and Ommer, B. High-resolution image synthesis with latent diffusion models. In *CVPR*, 2022b.
- Saharia, C., Chan, W., Saxena, S., Li, L., Whang, J., Denton, E. L., Ghasemipour, S. K. S., Ayan, B. K., Mahdavi, S. S., Lopes, R. G., Salimans, T., Ho, J., Fleet, D. J., and Norouzi, M. Photorealistic text-to-image diffusion models with deep language understanding. *NeurIPS*, 2022.

- Shang, Y., Yuan, Z., Xie, B., Wu, B., and Yan, Y. Post-training quantization on diffusion models. In *CVPR*, 2023.
- Song, J., Meng, C., and Ermon, S. Denoising diffusion implicit models. In *ICLR*, 2021. URL <https://arxiv.org/abs/2010.02502>.
- Sun, Y., Liu, R., Bai, H., Bao, H., Zhao, K., Li, Y., Hu, J., Yu, X., Hou, L., Yuan, C., et al. Flatquant: Flatness matters for llm quantization. *arXiv preprint arXiv:2410.09426*, 2024.
- Team, Z.-I. Z-image: An efficient image generation foundation model with single-stream diffusion transformer. *arXiv preprint arXiv:2511.22699*, 2025.
- Wan, T., Wang, A., Ai, B., Wen, B., Mao, C., Xie, C.-W., Chen, D., Yu, F., Zhao, H., Yang, J., Zeng, J., Wang, J., Zhang, J., Zhou, J., Wang, J., Chen, J., Zhu, K., Zhao, K., Yan, K., Huang, L., Feng, M., Zhang, N., Li, P., Wu, P., Chu, R., Feng, R., Zhang, S., Sun, S., Fang, T., Wang, T., Gui, T., Weng, T., Shen, T., Lin, W., Wang, W., Wang, W., Zhou, W., Wang, W., Shen, W., Yu, W., Shi, X., Huang, X., Xu, X., Kou, Y., Lv, Y., Li, Y., Liu, Y., Wang, Y., Zhang, Y., Huang, Y., Li, Y., Wu, Y., Liu, Y., Pan, Y., Zheng, Y., Hong, Y., Shi, Y., Feng, Y., Jiang, Z., Han, Z., Wu, Z.-F., and Liu, Z. Wan: Open and advanced large-scale video generative models. *arXiv preprint arXiv:2503.20314*, 2025.
- Wu, J., Wang, H., Shang, Y., Shah, M., and Yan, Y. Ptq4dit: Post-training quantization for diffusion transformers. In *NeurIPS*, 2024.
- Wu, J., Li, Z., Hui, Z., Zhang, Y., Kong, L., and Yang, X. Quantcache: Adaptive importance-guided quantization with hierarchical latent and layer caching for video generation. *arXiv preprint arXiv:2503.06545*, 2025a.
- Wu, J., Li, Z., Qin, H., Liu, X., Kong, L., Zhang, Y., and Yang, X. Flashedit: Decoupling speed, structure, and semantics for precise image editing. *arXiv preprint arXiv:2509.22244*, 2025b.
- Xiao, G., Lin, J., Seznec, M., Wu, H., Demouth, J., and Han, S. SmoothQuant: Accurate and efficient post-training quantization for large language models. In *ICML*, 2023.
- Yang, K., Zhang, X., Qin, H., Lin, Y., Yang, K., Yan, X., and Zhang, Y. Robuq: Pushing dits to w1. 58a2 via robust activation quantization. *arXiv preprint arXiv:2509.23582*, 2025.
- Zhao, T., Fang, T., Liu, E., Rui, W., Soedarmadji, W., Li, S., Lin, Z., Dai, G., Yan, S., Yang, H., Ning, X., and Wang, Y. Vudit-q: Efficient and accurate quantization of diffusion transformers for image and video generation. In *ICLR*, 2025.